Aerospace Science and Technology 116 (2021) 106869

Contents lists available at ScienceDirect

Aerospace Science and Technology

www.elsevier.com/locate/aescte

Dual-convolutional neural network based aerodynamic prediction and multi-objective optimization of a compact turbine rotor

Yuqi Wang [a,1], Tianyuan Liu [b,1], Di Zhang [a,*], Yonghui Xie [b]

[a] MOE Key Laboratory of Thermo-Fluid Science and Engineering, School of Energy and Power Engineering, Xi'an Jiaotong University, Xi'an, China
[b] Shaanxi Engineering Laboratory of Turbomachinery and Power Equipment, School of Energy and Power Engineering, Xi'an Jiaotong University, Xi'an, China

ARTICLE INFO

Article history:
Received 15 January 2021
Received in revised form 5 April 2021
Accepted 28 May 2021
Available online 5 June 2021
Communicated by Zhao Dan

Keywords:
Aerodynamic prediction
Multi-objective optimization
Turbine
Deep learning
Convolution neural network

ABSTRACT

With the development of neural network technology, surrogate models and dimensionality reduction strategies based on machine learning have become the research hotspots of aerodynamic shape optimization recently. In order to further improve the accuracy and interpretability of the traditional surrogate models, this research establishes a deep learning model, named Dual Convolutional Neural Network (Dual-CNN) for the aero-engine turbines. The aerodynamic performances are predicted and the pressure, temperature fields are reconstructed for multiple rotor profile conditions. The prediction of efficiency is compared with the accuracy of Gaussian Process Regression (GPR) and Artificial Neural Network (ANN) models. The results show that the proposed Dual-CNN model can accurately reconstruct the fields, thus interpreting the mechanism for the change of aerodynamic performance. Dual-CNN is more accurate than GPR and ANN in predicting efficiency and torque, whose error is within an acceptable range of optimization. Then, efficiency and torque are selected as the objective functions to perform a gradient-based multi-objective optimization by the automatic differentiation method and a Pareto solution is obtained. The trained Dual-CNN provides rapid and accurate prediction of performance without CFD calculation in the optimization. Finally, the sensitivity to train size is analyzed for the Dual-CNN model, which indicates that the sampling of 1500 cases for eight design variables in this dataset enables Dual-CNN to achieve favorable effect of field reconstruction and performance prediction.

1. Introduction

In recent years, the research on aerodynamic shape optimization has attracted more and more attention. The optimization methods can be divided into two types, namely, gradient-based method and gradient-free method [1]. A representative gradient-based method is the adjoint method, which needs to construct Reynolds-averaged Navier-Stokes (N-S) equation to solve the optimization problem [2–4]. In this case, it only needs to complete one convergence calculation, which results in a fast optimization speed [5,6]. Kenway et al. [7] presented a multipoint high-fidelity aerostructural optimization of an aircraft configuration. The gradients were computed by coupled adjoint sensitivity method with respect to hundreds of aerodynamic shape and structural sizing variables. However, the derivation of the solver and the sensitivity analysis can be complex, which needs in-depth theoretical knowledge of aerodynamics, while the constructed equation may also have the problem of convergence difficulty [8]. For a multi-objective optimization problem, the adjoint method acquires multiple constructed equations [9]. Hence, the implementation process is rather complex.

Gradient-free method has unique advantages in aerodynamic shape optimization. The genetic algorithm [10,11], particle swarm optimization [12], simulated annealing algorithm [13] etc. have many applications. These algorithms do not need to explore the relationship between optimization variables and objective function in the process, which corresponds to less demand for computational fluid dynamics (CFD) theoretical knowledge. Due to the fact that gradient-free method has to calculate multiple conditions with CFD method during the convergence process, it can be time-consuming [14,15]. To save the time of optimization process, Leifsson et al. [16] presented response surface surrogates and proposed the multi-objective evolutionary algorithm that works with a fast surrogate model obtained with kriging interpolation. The algorithm could be iteratively refined by local enhancements of the surrogate model. Toal et al. [17] accelerated the optimization process by the application of a multilevel cokriging model. They realized

* Corresponding author.
E-mail address: zhang_di@mail.xjtu.edu.cn (D. Zhang).
[1] These authors contributed equally to this paper.

https://doi.org/10.1016/j.ast.2021.106869
1270-9638/

Nomenclature

B	Bezier curve
C	primary function of Bezier curve
$\mathbf{f}$	field parameters
h	enthalpy ..... J/kg
$\dot{m}$	mass flow ..... kg/s
n	order of Bezier curve
P	output power ..... W
r	rotation speed ..... r/min
S	generalized source term
T	torque ..... N·m
$\boldsymbol{u}$	velocity vector ..... m/s
w	importance proportion in optimization
x	control points
$\mathbf{x}$	profile parameters
X	true value of objective function
X'	predicted value of objective function
$\mathbf{y}$	target of optimization

Greek symbols

α	update step in optimization
η	efficiency ..... %
ρ	density ..... kg/m^{-3}
φ	universal variable
$\boldsymbol{\psi}$	performance parameters
Θ_1	learnable parameters of the field prediction network
Θ_2	learnable parameters of the performance prediction network
Γ	generalized diffusion coefficient

Subscripts

is	isentropic
opt	optimal
z	axial direction

the optimization of a transonic airfoil with a reduction in the total number of simulations. To further improve the precision and accelerate the optimization, the surrogate model and dimensionality reduction strategy based on machine learning has become a research hotspot in recent years.

With the development of deep learning and neural network, the aerodynamic shape optimization has covered many aspects such as airfoils, turbine blades and compressor blades. These applications have largely promoted the aerodynamic performance of aero-engines, including gas turbines and other kinds of turbomachinery [18–20]. Traditional method was the construction of an ANN as a surrogate model using a database containing N-S solutions for all previous designs [21,22]. More recently, Yao et al. [23] trained multiple CNN structures to learn the lift coefficients of the airfoils with various shapes in multiple flow Mach numbers, Reynolds numbers and attack angles. Compared with multi-layered perceptron solutions, their CNN model exhibited a competitive prediction accuracy with minimal constraints in geometric representation. Considering the performance prediction, the neural-network based analyses were also covered [23–25]. Marx et al. [26] presented a novel approach on predictive maintenance in form of a performance based classification method for high pressure compressor airfoils. The procedure featured machine learning algorithms that established a relation between the airfoil geometry and the associated aerodynamic behavior. In our previous works, Liu [27,28] proposed a deconvolutional neural network with some semi-supervised learning strategy to establish an end to end mapping from low-dimensional measurable information to full physical fields and performance characteristics of interest, which is capable of predicting fields with remarkable accuracy in heat and transfer problem.

Supercritical carbon dioxide (S-CO_2), as a new type of working fluid, has unique advantages when applied in a turbomachinery. S-CO_2 working fluid has low viscosity and high density [29], which corresponds to high thermal efficiency and compact structure for its core components, namely, turbines and compressors [30]. S-CO_2 Brayton cycle can be used in a combined cycle [31] and compact power plants [32], which can be useful in aero applications [33]. Meanwhile, S-CO_2 Brayton cycle is a single-phase cycle with little phase change process. Hence, there is no condenser needed and the number of valves is only one tenth of Rankine cycle. Due to the low temperature (compared with gas turbines), the conventional stainless-steel material can be used and the manufacturing cost is low. Since the above characteristics, S-CO_2 turbomachinery has a good prospect of aerospace engineering application. At present, the study mainly lies in the optimization of power cycle. Wang et al. [34] performed the parametric optimization design of a S-CO_2 power cycle and Deng et al. [35] conducted the multi-objective optimization of a S-CO_2 recompression Brayton cycle, both based on genetic algorithm and ANN. Turbine is the core component of power generation and its research is of great significance. Considering S-CO_2 as working fluid, an efficient and useful optimization method for the turbomachinery has not been reported.

Considering the shortcomings of the above-mentioned study, this research establishes the Dual-CNN model based on deep convolutional neural network. The rotor blade profile of a S-CO_2 centrifugal turbine is parameterized and 3000 sets of CFD sampling calculations and data preprocessing are completed. Then, the Dual-CNN is trained to reconstruct the pressure and temperature field and perform the aerodynamic prediction for multiple profile conditions. In terms of efficiency prediction, the accuracy of Dual-CNN model is compared with the traditional GPR model and ANN model. With efficiency and torque as the objective function, an automatic differentiation method is used to achieve rapid multi-objective optimization based on gradients. Finally, the sensitivity to train size is analyzed for the Dual-CNN.

This data-driven aerodynamic performance prediction and optimization framework for turbine blades introduce field reconstruction, which promotes the accuracy of predicting efficiency and torque. The Dual-CNN model expands the functions of traditional surrogate models and employs field reconstruction to overcome the inability of traditional surrogate models. The field reconstruction provides information to interpret the mechanism for the change of aerodynamic performance without CFD calculation. Meanwhile, the automatic differentiation method is used to achieve rapid optimization of performance parameters based on gradients. Traditional black-box surrogate models can only use heuristic optimization algorithms such as genetic algorithm and simulated annealing algorithm. The proposed method with Dual-CNN can further improve the efficiency of optimization with gradient-based algorithm. Aiming at a S-CO_2 turbomachinery, without solving N-S equations by CFD, the established Dual-CNN model can quickly distinguish the trans-critical region (where the pressure or temperature is lower than the critical point) by predicting pressure and temperature on the blade surface, and precisely predict the turbine performance to improve the accuracy of multi-objective optimization.

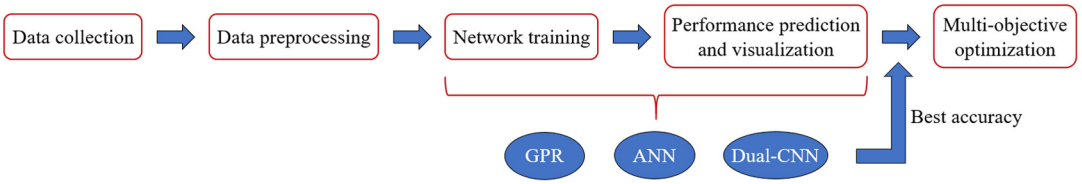

Fig. 1. Research process.

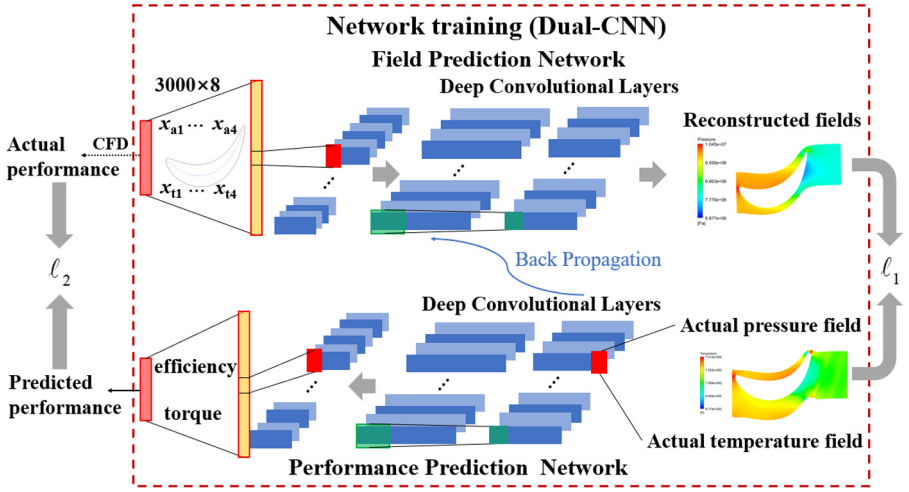

Fig. 2. Structure of Dual-CNN model. (For interpretation of the colors in the figure(s), the reader is referred to the web version of this article.)

2. Deep learning methods

Establishing the Dual-CNN-based deep learning is the core part of this research, with the functions to reconstruct the pressure and temperature fields as well as predict the efficiency and torque. In this section, we first introduce the overall framework of the research. The establishment and concrete parameters of Dual-CNN is then presented. To compare its validity, GPR and ANN models are also introduced and trained. It is worth mentioning that all experiments are carried out in the Python compiling environment using an Intel Core-i7 CPU and GTX 1660-Ti GPU. All the hyperparameters of models have undergone tedious tuning by random search and grid search to ensure an optimal performance.

The overall framework of the research is shown in Fig. 1. The first step is to collect the data required for the network training. A parameterization is conducted for the rotor blade profile of a S-CO_2 centrifugal turbine model. The second step is the data preprocessing. The field and performance data of each profile condition is extracted from the CFD results and preprocessed to serve as the input of models. The CFD performance and fields are considered as the actual value in the subsequent analysis. Available experimental data can also serve as the training input. The third step is the network training of GPR, ANN, and Dual-CNN with the corresponding performance prediction and visualization. The accuracy of Dual-CNN, GPR and ANN are compared and the prediction errors are analyzed. The model with best accuracy is used to perform the subsequent multi-objective optimization.

2.1. Dual-CNN model and optimization method

Deep CNN was originally proposed and applied by Zelier et al. [36,37]. The Dual-CNN model in this research is composed of a deep CNN-based field prediction network and a performance prediction network, as shown in Fig. 2. The input of the field prediction network is a matrix formed by 8 Bezier control points corresponding to a certain profile. After the linear and multiple deep convolution layers, the output is the reconstructed fields, which are the pressure and temperature information of 512 points at the intersection of the blade surface and the mid-span. The input of the performance prediction network is, the actual value of pressure and temperature fields with location information. After multiple deep convolutional, pooling, and linear layers, the isentropic efficiency and torque are predicted. Meanwhile, the gradient in this network is backpropagated. This model extends the functions of traditional surrogate models and can interpret the performance change by the field reconstruction. For the S-CO_2 turbomachinery, the Dual-CNN model can quickly determine the trans-critical area on the blade surface.

The reconstructed and actual fields are adopted to calculate the loss function of field prediction network (ℓ_1) while the predicted and actual performance are used to calculate the loss function of performance prediction network (ℓ_2). The input of the field prediction network is the profile parameters $\mathbf{x}$, and the output is the reconstructed pressure and temperature fields. The input of the performance prediction network is the actual fields $\mathbf{f}$, and the output is the predicted isentropic efficiency and torque for a certain profile. This process can be defined as follows:

$$\begin{aligned} \hat{\mathbf{f}} &= \hat{\mathbf{F}}_1(\mathbf{x}; \Theta_1) \\ \hat{\psi} &= \hat{\mathbf{F}}_2(\mathbf{f}; \Theta_2) \end{aligned} \tag{1}$$

Where $\hat{\mathbf{f}}$ is the reconstructed fields, $\hat{\psi}$ is the predicted performance parameters, Θ_1 is the learnable parameters of the field prediction network, Θ_2 is the learnable parameters of the performance prediction network. The training processes of these two networks are expressed as follows:

$$\Theta_1 = \arg\min_{\Theta_1} \left\{ \mathbf{E}_{(\mathbf{x},\mathbf{f})\sim D}(\ell_1) \right\} \tag{2}$$

$$\Theta_2 = \arg\min_{\Theta_2} \left\{ \mathbf{E}_{(\mathbf{f},\psi)\sim D}(\ell_2) \right\} \tag{3}$$

Where, $(\mathbf{x},\mathbf{f})\sim D$ indicates the profile parameters and the actual field parameters in defined domain D, ℓ_1 corresponds to the loss

Table 1
Structure of Dual-CNN.

Field prediction network		Performance prediction network	
Network type	Tensor output size	Network type	Tensor output size
Input	32 × 8 (profile parameters)	Interpolation	32 × 2 × 512 (field parameters)
Linear	32 × 1 × 2048	Conv1d	32 × 64 × 256
Conv1d × 4	32 × 128 × 16	Conv1d	32 × 128 × 128
Conv1d × 4	32 × 128 × 32	Conv1d	32 × 256 × 64
Conv1d × 4	32 × 128 × 64	Conv1d	32 × 512 × 32
Conv1d × 4	32 × 128 × 128	Conv1d	32 × 1024 × 16
Conv1d × 4	32 × 128 × 256	Conv1d	32 × 2048 × 8
Conv1d × 4	32 × 128 × 512	Conv1d	32 × 4096 × 4
Output Conv1d	32 × 2 × 512	AvgPool1d	32 × 4096 × 1
		Linear	32 × 512
			32 × 2

function of the field prediction network. $(\mathbf{f},\boldsymbol{\psi})\sim D$ indicates the actual field and performance parameters in domain D, and ℓ_2 corresponds to the loss function of the performance prediction network.

Adaptive momentum estimation optimization algorithm (Adam) [38] is used as the optimizer during the training process for both field prediction network and performance prediction network. The learning rate is first set to 0.003. After 100 epochs of training, the learning rate decreased to one tenth of the original in each 50 steps. Both the loss functions ℓ_1 and ℓ_2 adopt SmoothL1Loss in PyTorch [39]. After hundreds of epochs, the loss function is reduced to a minimum, thus completing the training of Dual-CNN. The division of training set and validation set will be discussed later. The concrete structure of Dual-CNN with the training batch size 32 is presented in Table 1. In the field prediction network, each convolution layer includes 4 convolution sub-modules, which contains a convolution kernel (kernel size = 3, padding = 1, stride size = 1, input and output channels are 128) and LeakyReLU activation function. In the performance prediction network, each convolutional layer contains a convolution kernel (kernel size = 3, padding = 1, stride size = 2) and ReLU activation function. Total trainable parameters of 1,201,922 with size 4.58 MB and 35,653,442 with size 136.01 MB are adopted for field prediction network and performance prediction network respectively.

The optimization process aiming at the performance parameters $\boldsymbol{\psi}$ is shown in Eq. (4). The automatic differentiation method based on gradient is adopted as optimization algorithm to obtain the profile parameters $\mathbf{x}$ which possesses the maximum isentropic efficiency η_{is} and torque T_z.

$$\mathbf{x}_{\text{opt}} = \arg\max_{\mathbf{x}} \{\boldsymbol{\psi}\} = \arg\max_{\mathbf{x}} \{\eta_{\text{is}}, T_z\} \tag{4}$$

In the optimization process, the established Dual-CNN is used to obtain the performance parameters of each profile. We conduct a multi-objective optimization with a simple gradient-based algorithm utilized in multi-task deep learning [40]. The target of the optimization is defined as $\mathbf{y}$ in the following Eq. (5). The optimization variable $\mathbf{x}$ can be easily updated based on the gradient with the automatic differentiation tool.

$$\begin{aligned} \mathbf{y} &= w \times \hat{\boldsymbol{\psi}}\{\eta_{\text{is}}\} + (1-w) \times \hat{\boldsymbol{\psi}}\{T_z\} \\ \mathbf{x} &= \mathbf{x} + \alpha \cdot \nabla_{\mathbf{x}}\mathbf{y} \end{aligned} \tag{5}$$

Where w is the importance proportion in optimization. When $w = 1$, efficiency is only considered as objective in the optimization while $w = 0$, torque is only considered. The approximate Pareto-optimal front can be obtained with the value of w set from 0 to 1 with an interval of 0.1. It should be emphasized that the all the performance parameters in Eq. (5) are normalized to a standard interval. A factor α to control update step is set as 0.1 in this research. The corresponding optimal target of each w is obtained by 100 calculations based on Dual-CNN rather than CFD method. Hence, after eleven optimization calculations, the Pareto solution is rapidly obtained.

2.2. GPR model

In the traditional machine learning methods without field prediction, the established surrogate models directly learn the mapping relationship from design variables to performance parameters, as shown in Eq. (6).

$$\hat{\boldsymbol{\psi}} = \hat{\mathbf{F}}(\mathbf{x}; \Theta) \tag{6}$$

Both GPR and ANN model adopt this mapping relationship. In the GPR model, we use variational and approximate Gaussian processes based on Bayesian Deep learning [41]. This model is commonly used when the GP likelihood is non-Gaussian (e.g. for classification) or Gaussian (e.g. for regression) and when we need to scale up GP regression by using stochastic optimization or use GPs as part of larger probabilistic models. With GPyTorch [42] it is possible to implement various types of approximate GP models.

A batch variational GP is constructed using a Cholesky Variational Distribution and a Variational Strategy. Each of the batch dimensions corresponds to one of the outputs. In addition, we wrap the variational strategy to make the output appear as a Multitask Multivariate Normal distribution. The Cholesky Variational Distribution, mean module, and covariance modules are marked as batch to ensure that we learn a different set of variational parameters and hyperparameters for each output dimension.

In the training process, we choose Adam as the optimizer and variational evidence lower bound (ELBO) as the loss object. A radial basis function (RBF) kernel is used and the Cholesky Variational Distribution with inducing points = 256 is applied. The learning rate is set as 0.05.

2.3. ANN model

The ANN model also establishes a mapping relationship as shown in Eq. (6). The presented ANN model contains three linear layers with activation function and dropout. The input is 8 profile parameters. The middle two linear layers output 512 neurons with ReLU as activation function. The last linear layer outputs the predicted efficiency. A dropout 0.05 strategy is used to avoid overfitting for the middle two linear layers. The optimizer adopts Adam. Adam algorithm combines the advantages of Adagrad to handle sparse gradients and RMSprop to handle non-stationary targets. It requires less memory requirements and has different adaptive learning rates for different parameters. It is suitable for most non-convex optimizations as well as large datasets and high-dimensional space. The *MSEloss* in PyTorch [39] is used as the loss function, and the calculation method is defined as follows:

$$MSEloss = \frac{1}{N}\sum_{i=0}^{N}(X_i' - X)^2 \tag{7}$$

Where X is the true value of the objective function and X' is the predicted output by the ANN. The initial learning rate is 0.05. After training for 100 steps, the learning rate decreases to one-tenth of the original in every 50 steps.

3. Data collection and preprocessing

The high density of the S-CO_2 working fluid results in the small flow area and blade height. Hence, straight blades are usually used in the design. For the studied model, we simplify the blade profile

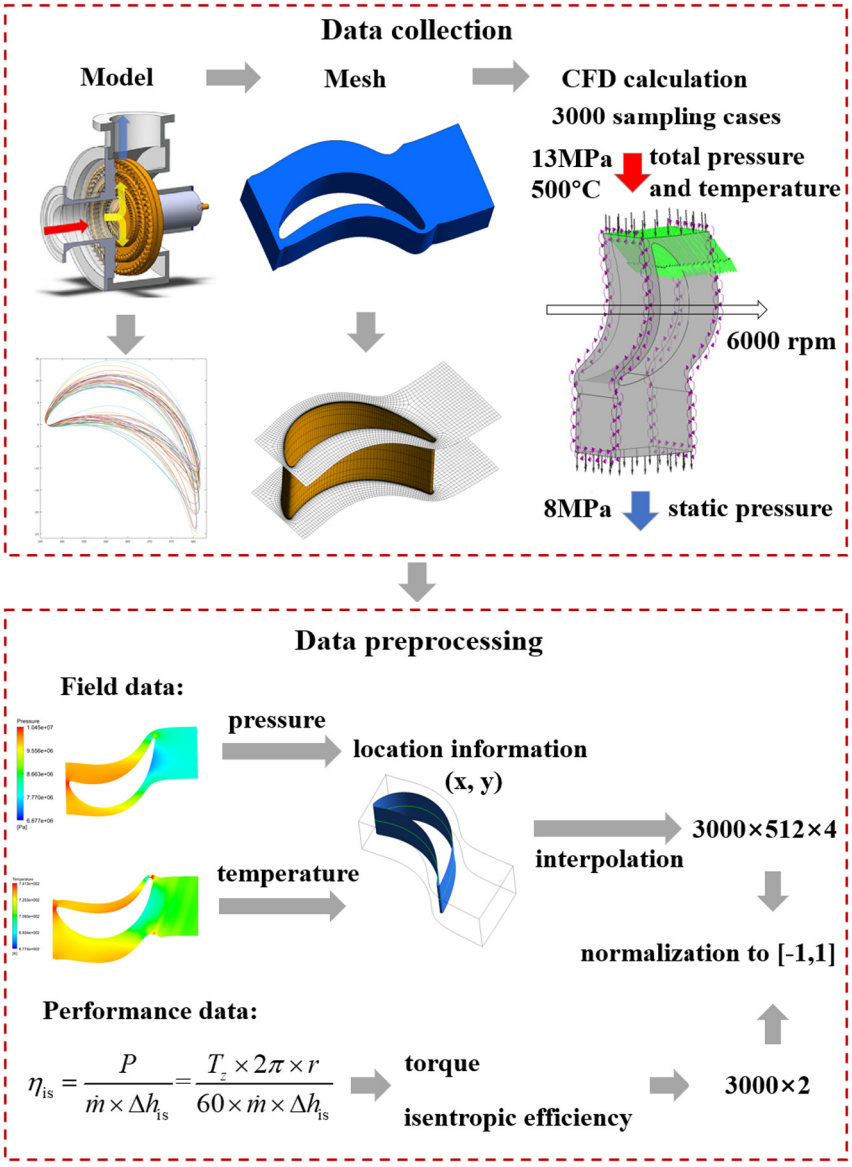

Fig. 3. Process of data collection and preprocessing.

to two dimensions, which helps to reduce the number of variables in the sampling, and facilitates the establishment of subsequent data-driven prediction networks and the development of optimization research. The process of data collection and preprocessing is shown in Fig. 3. Latin Hypercube Sampling method is used to generate 3000 sets of blade profiles. The commercially available software CFX 15.0 is used for numerical calculation. Macro commands are called in Matlab to complete the mesh generation in TurboGrid and the numerical simulation in CFX 15.0. The field data and aerodynamic performance of each case are obtained by solving the compressible viscous steady N-S equation for the three-dimensional fluid domain of the turbine. The field data are the pressure and temperature information at the intersection of the blade surface and the mid-span combined with x and y coordinates of each point. The data are interpolated to form a 3000 × 512 × 4 matrix, where 3000 × 512 × 2 with pressure and temperature is used for the training of performance prediction network. x and y coordinates are used for postprocessing. The performance data containing torque and isentropic efficiency are interpolated to form a 3000 × 2 matrix.

3.1. Research model and parametrization

The S-CO_2 centrifugal turbine model is derived from the design of Luo et al. [43]. The flow channel parameters of rotor blade for the single-stage turbine is obtained from the reference and not listed in detail due to space limitation. In this research, the rotor blade profile is parameterized based on Bezier curves. The curve $B(t)$ and primary function $C_{n,i}(t)$ of a n-order Bezier curve can be expressed as follows:

$$B(t) = \sum_{i=0}^{n} C_{n,i}(t)\, x_i$$
$$C_{n,i}(t) = \frac{n!}{i!\,(n-i)!} t^i (1-t)^{n-i} \tag{8}$$

Specially, the blade profile is defined by the distribution of thickness and the blade angle to radial direction of the mean-line. For each distribution, four control points are selected to form the Bezier curve, as shown in the following Fig. 4. A cubic Bezier curve is adopted for four control points, and the equation of the profile can be written as:

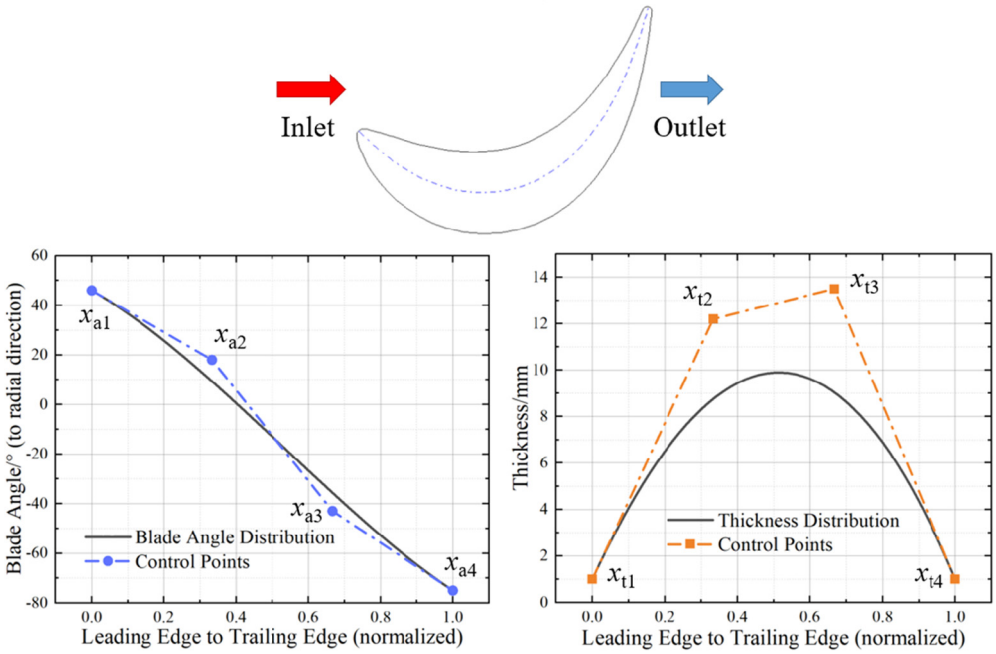

Fig. 4. Parameterization of the rotor blade.

$$B(t)=\sum_{i=1}^{4} C_{3,i}(t)\,x_i = x_1(1-t)^3 + 3x_2 t(1-t)^2 + 3x_3 t^2(1-t) + x_4 t^3,\ t\in[0,1] \tag{9}$$

Where, x represents the control points, and B corresponds to the distribution curves calculated from the control points. For each blade profile, the blade angle distribution and thickness distribution from the leading edge to the trailing edge are obtained from the eight control points x given in Fig. 4. Then, the modeling of the fluid domain can be completed.

3.2. Governing equations and boundary conditions

The governing equation comes from the conservation of mass, momentum and energy. With regard to a steady-state simulation, a general form can be written as:

$$\mathrm{div}(\rho \boldsymbol{u}\varphi) = \mathrm{div}(\Gamma\,\mathrm{grad}\,\varphi) + S \tag{10}$$

The three terms in the equation are convection, diffusion and source term, respectively. Among them, φ is the universal variable, and $\varphi = 1$ means continuity equation. It represents the energy equation when φ is temperature. The momentum equation is indicated when φ is applied as velocity of arbitrary direction. Γ and S are generalized diffusion coefficient and generalized source terms, respectively.

CFX uses the Reynolds Averaged Navier-Stokes (RANS) equation to deal with turbulent flow and the finite volume method is adopted for discretization. According to our previous research [44], aiming at the radial turbine, SST k-w turbulence model accord with the experimental data most precisely compared to k-ε, RNG k-ε and k-w turbulence models. Hence, SST k-w turbulence model is used in the CFD sampling process to generate an accurate dataset. The hexahedral mesh in the fluid domain is generated using TurboGrid. The hub, shroud and blade wall have been densely generated to satisfy the y^+ recommended by the turbulence model. The solid walls adopt adiabatic and no-slip boundary conditions. For this S-CO_2 centrifugal turbine model, the boundary conditions are given in Fig. 3.

Table 2
Results of mesh independence test.

Mesh scheme	Total element number/10^4	Output power/MW	Relative error/%	Isentropic efficiency/%	Relative error/%
1	2.7	11.16	/	93.23	/
2	4.7	11.10	−0.54	93.11	−0.13
3	9.3	11.10	0	93.10	−0.01
4	14.4	11.09	−0.09	93.12	0.02

3.3. Validation of fluid property and grid

Accurate simulation of S-CO_2 properties is vital in the numerical calculation of this model. In this study, a widely used real gas property (RGP) format table is adopted, and parameters such as density, enthalpy and entropy of the working fluid at a certain temperature and pressure are input into CFX. The input data are derived from NIST Refprop 9.1. The predefined pressure range is 6-15 MPa with gradient 0.2 MPa and the temperature range is 500-800 K with gradient 5 K, in order to adapt to the convergence process. The RGP table is generated in MATLAB and input into CFX by TASCflow RGP method. The properties of S-CO_2 are calculated by bilinear interpolation in CFX. The accuracy of the RGP table has been verified in the work of Odabaee et al. [45] and Kim et al. [46].

In the calculation of each case, a high-quality hexahedral mesh is generated for the fluid domain of different rotor profile by the batch mode in TurboGrid. O-type mesh is used around the blade to ensure high quality of the leading and trailing edges. Taking into account the periodic symmetry of the turbomachinery model, a single-channel of the rotor blade is adopted to save the calculation time of each case. The grid-independence verification of the single-channel model is conducted and the results are shown in Table 2.

From the above table, the relative error of the output power of four mesh schemes is less than 0.6% and the relative error of isentropic efficiency is less than 0.2%. Therefore, in order to save the computation time, we chose the mesh scheme 2 to conduct the initial sampling. The mesh of the simulation domain for the sampling of the rotor blade example is shown in the Fig. 3.

Table 3
Ranges of sampling.

Parameters	x_{a1}	x_{a2}	x_{a3}	x_{a4}	x_{t1}	x_{t2}	x_{t3}	x_{t4}
Ranges	35 ~ 55	−5 ~ 15	−45 ~ −25	−80 ~ −60	0.5 ~ 2	10 ~ 15	10 ~ 15	0.5 ~ 2

3.4. Dataset and evaluation criterion

As the input of Dual-CNN, GPR and ANN, 3000 sets of CFD calculations are performed first. The eight parameters of the rotor blade profile are sampled by Latin hypercube sampling method. After multiple tests, we select the sampling ranges where the CFD simulations can mostly converge. The ranges are shown in Table 3.

In the multi-objective optimization, we adopt output torque and isentropic efficiency as the objective function for the evaluation of the aerodynamic performance. The discussed isentropic efficiency and output torque are defined as the following equation:

$$\eta_{is} = \frac{P}{\dot{m} \times \Delta h_{is}} = \frac{T_z \times 2\pi \times r}{60 \times \dot{m} \times \Delta h_{is}} \tag{11}$$

Where P is the output power, T_z stands for the torque towards z axis. Hence, T_z is in direct proportion to P and it can be used to measure the power capacity. r represents the rotational speed, Δh_{is} is the isentropic enthalpy drop during the expansion process and $\dot{m}$ is mass flow rate.

4. Results and discussion

In the above sections, a data-driven aerodynamic performance prediction and optimization framework for aero-turbine blades is established. The sampling and preprocessing of a S-CO_2 centrifugal turbine are completed. Based on the sampling data, the training of Dual-CNN, GPR and ANN introduced in section 2 are completed. First, the results of field reconstruction and aerodynamic prediction for the Dual-CNN model are given and the accuracy of the three models are compared. Then, multi-objective optimization and sensitivity to train size based on the most accurate Dual-CNN are studied. The optimization algorithm adopts the automatic differentiation method based on the gradient. The trained Dual-CNN provides rapid and accurate prediction of performance without CFD calculation in the optimization. Besides, without solving the N-S equations in CFD, the established Dual-CNN model can quickly determine the trans-critical region on the blade surface by predicting pressure and temperature.

4.1. Aerodynamic prediction

The field reconstruction includes pressure and temperature field. During the training of the model, the prediction of isentropic efficiency and torque are completed at the same time. Fig. 5 respectively shows the variation of the loss function of field and performance prediction network with iteration steps during the training process. A batch size of 32 which can reach satisfactory accuracy is selected after multiple tests and each batch size is trained in each iteration. The ratio of the quantity of the training set to the validation set is 4:1.

From Fig. 5, the loss function drops extremely fast at the beginning. When the iteration step reaches 1500, with the gradual decrease of the learning rate, the loss function of the reconstructed field network drops below 10^{-5} on the train set while it drops to around 10^{-4} on the validation set. In the prediction network of the isentropic efficiency and torque, the loss function on the train set drops to about 10^{-5} while it drops to about 10^{-4} on the validation set. Hence, the training process of the networks is considered completed.

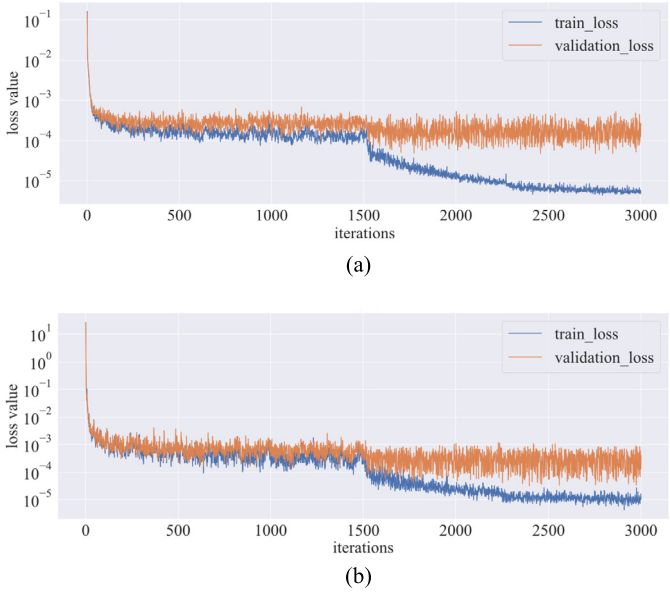

Fig. 5. Training Process (a: field prediction network; b: performance prediction network).

Fig. 6 shows the comparison of the reconstructed fields with the real field distribution. The pressure and temperature distributions of the intersection of the blade surface and the mid-span are reconstructed respectively.

From Fig. 6, the predictions of pressure and temperature are similar to the actual field. The accuracy of the Dual-CNN model is guaranteed. Along the flow direction, the pressure and temperature gradually decrease. The pressure distribution can indicate the power capacity of the blade. For the pressure distribution in Fig. 6(a), the distribution of the leading edge and trailing edge are partially enlarged. In the low-pressure region of the leading edge, the predicted pressure is slightly lower than the actual pressure while the predicted pressure in the high-pressure zone is slightly higher than the actual pressure at the trailing edge. Generally, the error of the prediction at the suction surface and pressure surface in the middle section of the blade is rather small. From the predicted pressure distribution, the location of the trans-critical area where the pressure is below critical pressure 7.38 MPa can be further predicted for each blade profile condition, as shown below the red line. From Fig. 6(b), it can also be found that the larger prediction errors of temperature are located at the leading and trailing edge of the blade with larger gradients. It is relatively accurate in the middle section.

For the performance prediction network, Fig. 7 selects all data in the validation dataset to present the prediction effect. The predicted vs actual efficiency and the relative error with its distribution density are presented.

As can be seen in Fig. 7(a), the predicted isentropic efficiency is close to the actual value. All scatters of validation dataset fall within the 1% interval near y = x line. In the high efficiency region (when the efficiency is greater than 94%), the predicted scatters are the closest to the y = x line, indicating that this model is credible for the subsequent optimization. In Fig. 7(b), it can be concluded that the absolute value of the maximum relative error

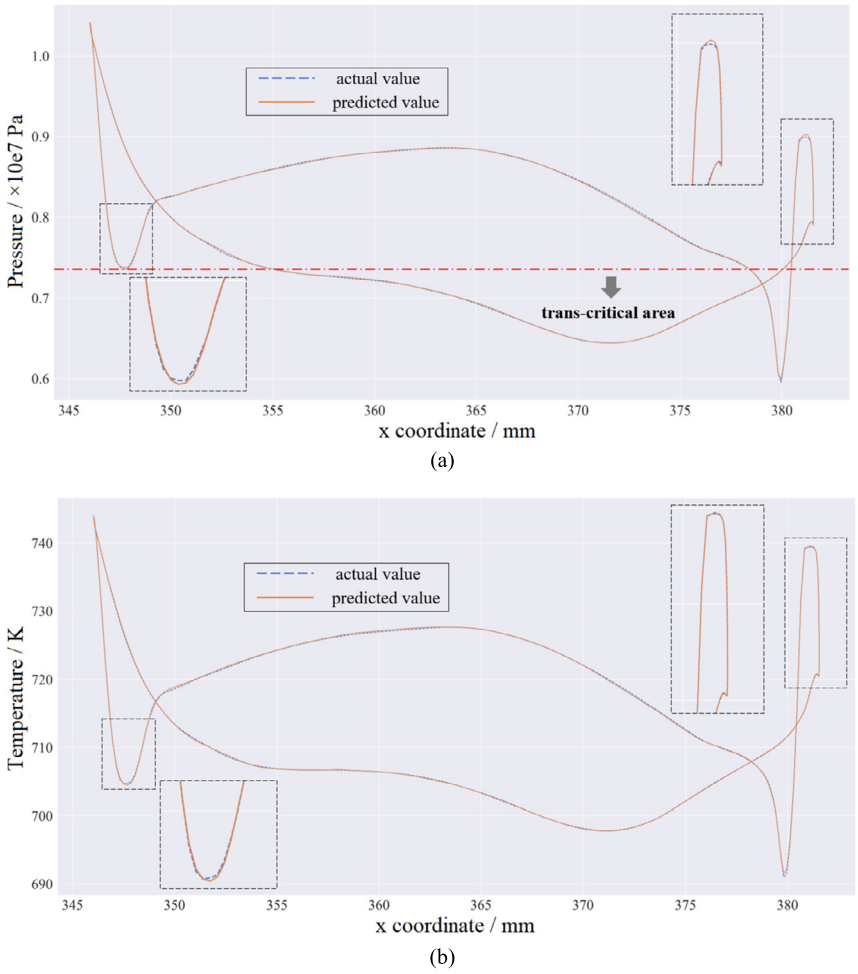

Fig. 6. Reconstructed fields (a: pressure; b: temperature).

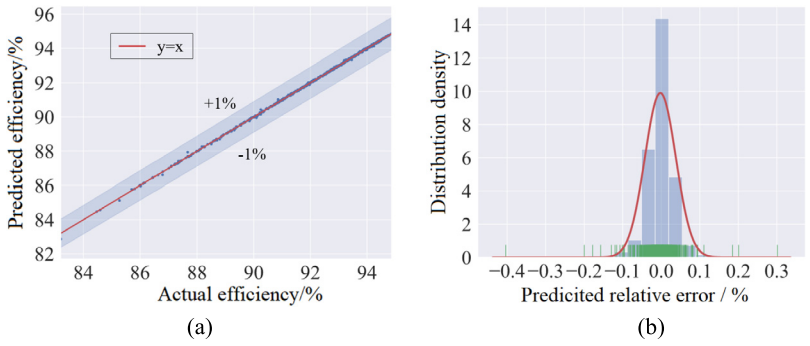

Fig. 7. Predicted efficiency of Dual-CNN (a: predicted vs actual; b: distribution density of relative error).

is less than 0.5%. The distribution density basically conforms to the normal distribution. Therefore, this network is reliable for predicting isentropic efficiency.

Likewise, Fig. 8 gives the predicted vs actual torque with predicted scatters of all data in the validation dataset. The relative error with its distribution density is also presented.

In Fig. 8(a) and (b), the predicted torque falls within the 2% interval near y = x line, and the absolute value of the maximum relative error is less than 1.5% with an approximate normal distribution. Hence, this performance prediction network is practicable for predicting torque, thus obtaining the power of the turbine.

4.2. Comparison of accuracy

In this section, GPR model and ANN model are trained. The isentropic efficiency is selected to compare the accuracy with the Dual-CNN model. The most accurate model can be chosen for the subsequent optimization research. After several tests, a batch size of 512 is employed in the training process of GPR and ANN to ensure the effect. The ratio of the training data and the validation data is also 4:1. To perform the comparison, 1000 sets of sampling data are randomly selected to calculate the relative error of predicted efficiency. Fig. 9 shows the box plot with scatters of the relative error of predicted efficiency for the three models.

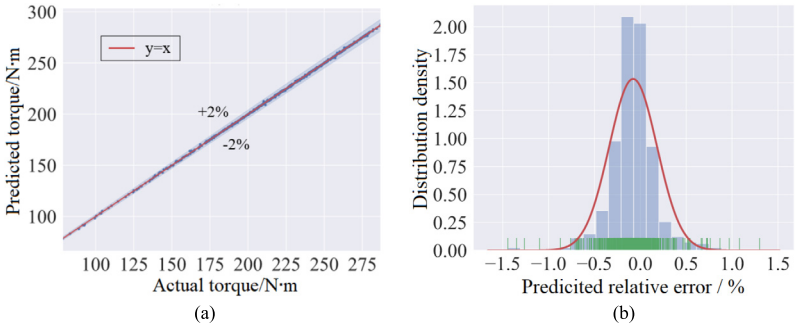

Fig. 8. Predicted torque of Dual-CNN (a: predicted vs actual; b: distribution density of relative error).

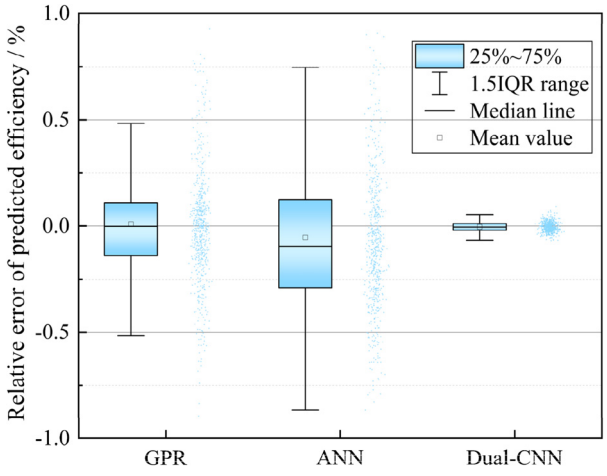

Fig. 9. Comparison of efficiency prediction effect.

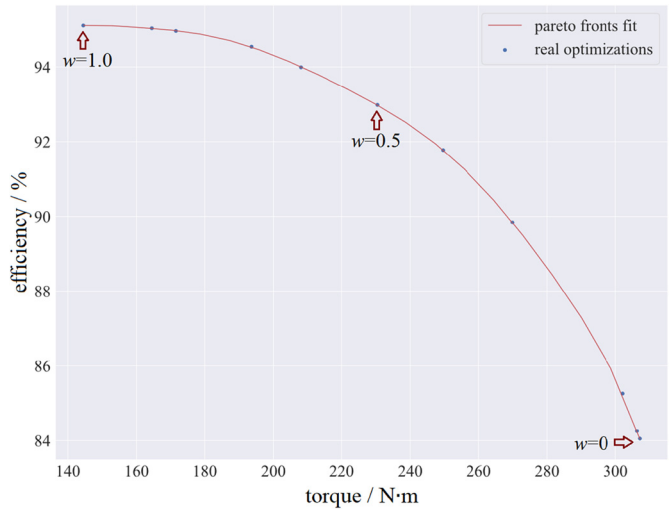

Fig. 10. Pareto solution of the multi-objective optimization.

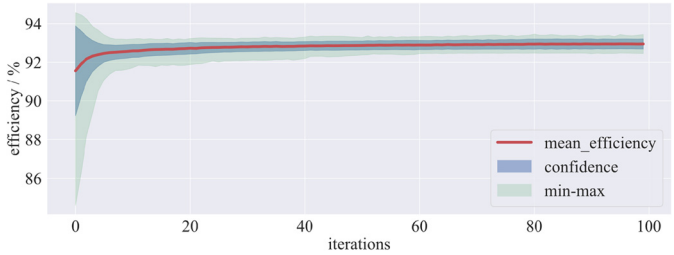

Fig. 11. Variation of efficiency with optimization iterations ($w = 0.5$).

The visualized error distribution between ± 1% of the efficiency prediction for the three models can be acquired from Fig. 9. As seen from Fig. 9, the relative error of predicted efficiency is the highest when applying ANN model and the absolute maximum error of 1.5 interquartile range for the efficiency prediction is close to 1%. Besides, the median line and mean value of ANN are obviously negative, which indicates the prediction of ANN is generally conservative. The 1.5 interquartile range of GPR is near 0.5% while the proposed Dual-CNN possesses the lowest relative error when predicting efficiency and its 1.5 interquartile range is approximately 0.1%. Moreover, the median lines of GPR and Dual-CNN are close to 0, which indicates the prediction of these two models is unbiased.

As stated by Forrester et al. [15], the accuracy requirement is rather subjective and it depends on the noise of the sampling data from the original model as well as the available computing resources. For turbomachinery, it can be considered as a significant promotion by 1 ∼ 2% for efficiency in the optimization research [11,18,19]. Hence, the GPR and ANN models are lacking in accuracy for the subsequent optimization research since multiple relative error of predicted scatters are close to 1%. The established Dual-CNN model with the best accuracy is employed in the optimization.

4.3. Multi-objective optimization

Based on the most accurate Dual-CNN model, multi-objective optimization is performed with isentropic efficiency and torque as the objective function. Each optimization point has 100 iteration steps and the obtained Pareto front fit is shown in Fig. 10, where the blue dots are the actual optimized profile conditions. From left to right, the w in Eq. (5) is from 1.0 to 0 with −0.1 as an interval. In other words, the importance of efficiency in optimization is 100% to 0% with −10% as the gradient. It can be found that as the torque increases, the optimal efficiency gradually decreases. This is because the mass flow rate required in high-power conditions increases faster than the power.

Taking the condition where efficiency and torque share respectively 50% importance in the optimization as an example, Fig. 11 shows the change in efficiency with the iteration steps. In Fig. 11, the red line is the average efficiency in each step, and the blue area is the confidence interval. The green region is the minimum and maximum efficiency in each iteration step. With the increase of iterative steps, the efficiency first increases rapidly and then tends to be flat. After 80 steps, the efficiency hardly increases with the iteration steps. Hence, we consider this optimization of $w = 0.5$ is completed.

As shown in Fig. 12, the black profile is the optimal case in each iteration step and the color gradually darkens as the iteration step increases. The blue profile is the worst efficiency condition in the sampling process while the green profile is the best. The red profile is the optimal case in the optimization that the efficiency and the

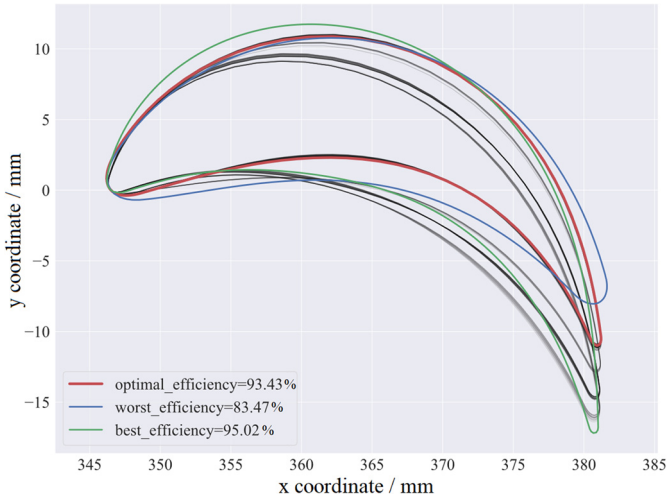

Fig. 12. Blade profiles during optimization process.

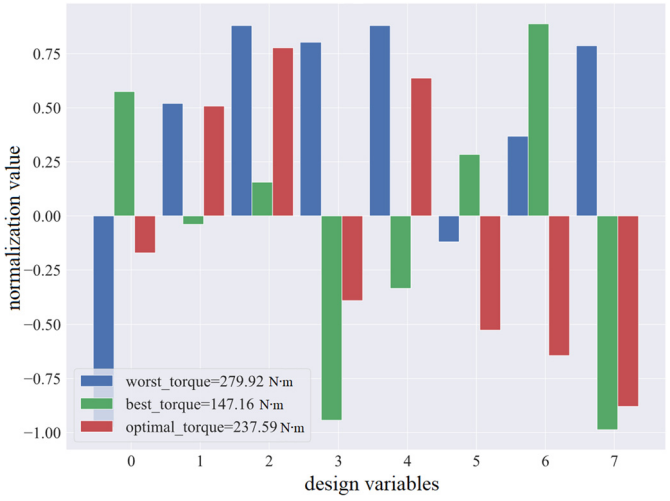

Fig. 13. Design variables of the optimal case and the sampling cases.

torque share respectively 50% importance. The best efficiency in sampling is 95.02%, the worst efficiency is 83.47%, and the optimal efficiency in this optimization case is 93.43%.

Fig. 13 presents the normalization values of 8 blade profile parameters of the optimal case in the optimization. Comparing the best profile and the worst profile in the initial sampling, the 8 blade profile parameters generally does not reach the extreme value in the normalized range of −1 to 1. The optimal blade profile parameters have the values between the best and worst conditions in the sampling, which indicates that the sampling range is reasonable. According to Equation (3), the torque of the best efficiency case in the sampling is 147.16 N·m, and the corresponding power output is 9.99 MW. The torque of the worst efficiency case in the sampling is 279.92 N·m, and the corresponding power is 18.99 MW. In the optimization that the efficiency and the torque share respectively 50% importance, the optimal profile corresponds to the torque 237.59 N·m and the power output 16.12 MW.

Fig. 14 gives the reconstruction results of the pressure field at the intersection line between the mid-span and the blade surface of the optimal case and the best and worst sampling cases. The density and specific heat of CO_2 near the critical point change sharply. Hence, reducing the trans-critical area is the key to a stable operation of S-CO_2 turbomachinery, especially for compressors [47]. For the worst efficiency case in the sampling, the streamwise pressure is relatively lower, and a larger trans-critical zone is generated on the blade surface and the flow region. The minimum pressure at the blade exit is as low as about 5 MPa so that it has low efficiency. However, the pressure difference between the suction surface and pressure surface is large, which corresponds to a large output power. For the best efficiency case in the sampling, the pressure of the blade surface is generally high, and there is almost no trans-critical area at the trailing edge of the blade, which corresponds to higher efficiency. Nevertheless, the pressure difference between the suction surface and the pressure surface at the blade inlet and the middle section is small. Hence, this case has lower power capacity. For the optimal profile when the efficiency and the torque share respectively 50% importance, compared with the best efficiency case, the pressure difference between the suction surface and the pressure surface increases. Hence, the power capacity is significantly enhanced and the trans-critical area at the trailing edge is also controlled within a smaller range, which results in a favorable efficiency.

4.4. Sensitivity to train size

An inherent characteristics of data-driven deep learning methods is that model quality strongly depends on the training data. Hence, it is significant to investigate the sensitivity to train size of the Dual-CNN. Specifically, the accuracy of performance parameters and field reconstruction are tested for the train size of 0.1, 0.3, 0.5, 0.65, 0.8, and 0.95 on the random 1000 sets of sampling data. It provides the basis for selecting train size of the Dual-CNN model. The parameter of train size is defined as the number of training samples divided by the total number of samples.

Fig. 15 presents the predicted mean error and standard deviation of efficiency and torque for different train size. Approximately, the predicted mean relative error of efficiency shows a decreasing trend with the increase of the train size and the decrease slows down when the train size is larger than 0.3. In practical applications, the size of the sampling dataset can be selected according to the prediction accuracy requirements. For the 1000 prediction cases, the mean predicted error of efficiency occurs when the train size is 0.8. The predicted mean relative error is 0.019% and the corresponding standard deviation is 0.016%, which indicates that the Dual-CNN model can substitute the CFD method and save the time cost in the optimization process for this model.

The predicted mean relative error of torque also shows a decreasing trend while the trend slows after the train size reaches 0.5. When the train size is 0.95, the predicted mean relative errors of the selected 1000 dataset and its standard deviation are the

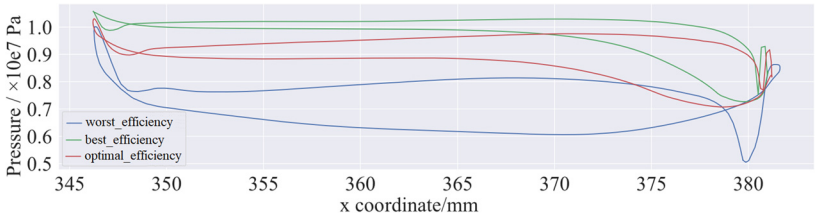

Fig. 14. Pressure distribution of the optimal case and the sampling cases.

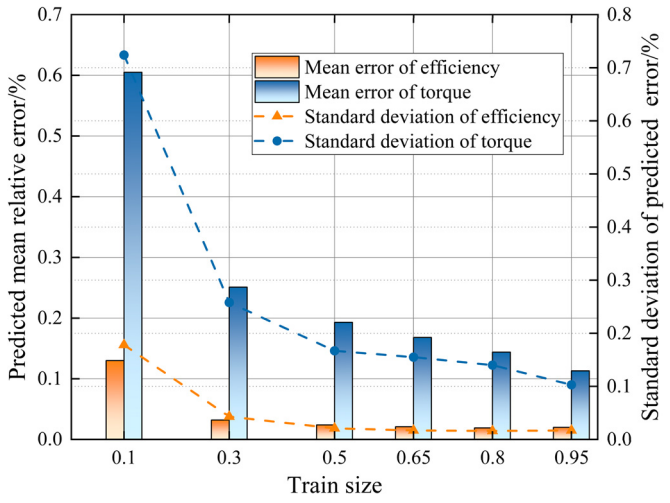

Fig. 15. Predicted mean error and standard deviation of performance for different train sizes.

smallest, which are 0.113% and 0.103% respectively. This indicates the increase of training data can further improve the prediction accuracy of torque. In practical applications, the number of sampling case for the training can be selected according to computation resources. In general, the Dual-CNN model presents a good effect when the data quantity of the training dataset reaches 1500 and can serve as an efficient analysis tool for the turbine performance instead of CFD software.

The train size also affects the accuracy of field reconstruction. Fig. 16 shows the predicted pressure distribution of different train size at the intersection line between the mid-span and the blade surface. For each train size, the predicted result of a certain profile at the end of the network training is compared with the actual value.

It can be seen from Fig. 16 that when the train size is 0.1 and 0.3, the predicted pressure distribution is quite different from the actual value. The predicted pressure in the middle of the suction and pressure surface is significantly higher than the actual pressure. When the train size is larger than 0.5, the predicted value at the middle section of the blade is more accurate. However, at positions of the leading edge and trailing edge where the pressure gradient is large, the train sizes of 0.5, 0.65 and 0.95 are not accurate enough. In general, when the train size is 0.8, the predicted pressure distribution is the closest to the actual value.

To further quantify the error of the reconstructed fields, the mean relative error (*MRE*) of predicted fields is introduced. *MRE* is defined as follows:

$$MRE = \frac{\sum_k \left| \frac{f_{P,T} - f'_{P,T}}{f_{P,T}} \right|}{k} \tag{12}$$

Where f and f' are respectively the actual and predicted field parameters, k is the selected grid node number of pressure or temperature, in this case, is 512. The *MRE* of 1000 cases are selected and analyzed. Fig. 17 gives *MRE* of both temperature and pressure fields for the six train sizes ranging from 0.1 to 0.95.

As shown in Fig. 17, when the training data set size is 0.1, the *MRE* of pressure and temperature are the highest and the maximum error of 1.2 interquartile range for predicted temperature and pressure reach up to 0.12% and 0.7% respectively. As the train size increases to greater than 0.5, the median lines and mean values of each prediction are all below 0.1%, which indicates the Dual-CNN is satisfying for field prediction when the train size is higher than 50% of the total 3000 samples. Especially when the train size is 0.8, the mean values of *MRE* are low. Besides, the *MRE* is relatively concentrated and the interquartile ranges are the smallest for pressure and temperature prediction.

5. Conclusion

Aiming at a compact turbine rotor for aerospace engineering application, the Dual-CNN model based on deep convolutional neural network is established. The prediction accuracy of this model is compared with GPR and ANN models. A multi-objective optimization based on gradients is then performed and the sensitivity to train size is studied. The established data-driven framework for turbine blades realizes rapid and accurate field reconstruction and performance prediction without CFD method for multiple profile conditions. The proposed Dual-CNN model expands the function of traditional surrogate models since it provides the field information to interpret the performance change and promote the prediction accuracy of performance parameters. With the proposed Dual-CNN model, a faster evaluation for the initial design and optimization stage and a real-time adjustment direction for the operation and maintenance stage can be acquired. The following conclusions are obtained:

(1) Dual-CNN can accurately predict the pressure and temperature distribution. Under the most accurate hyperparameters, the predicted value and the actual value have good consistency in

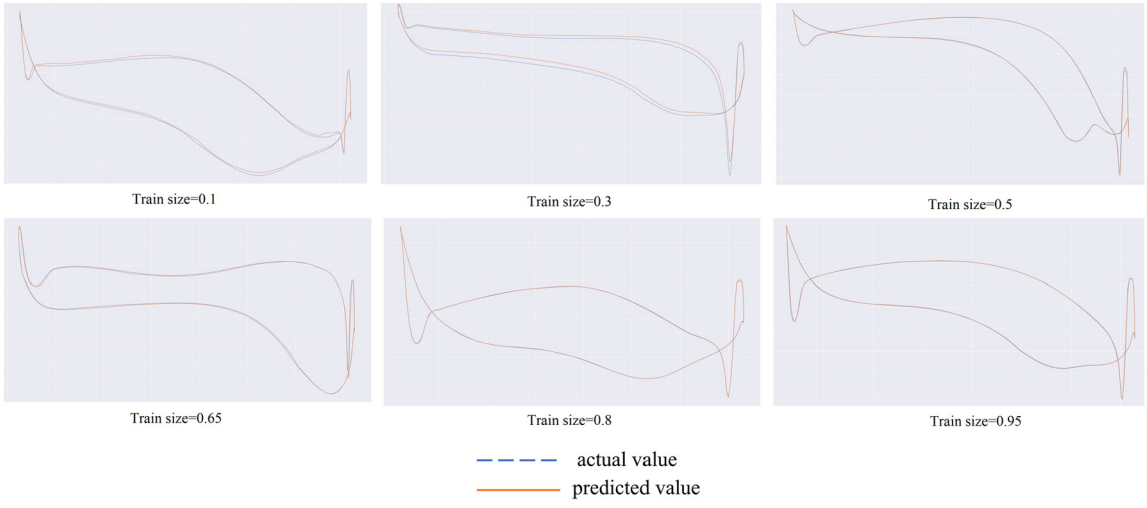

Fig. 16. Predicted pressure distribution of different train sizes.

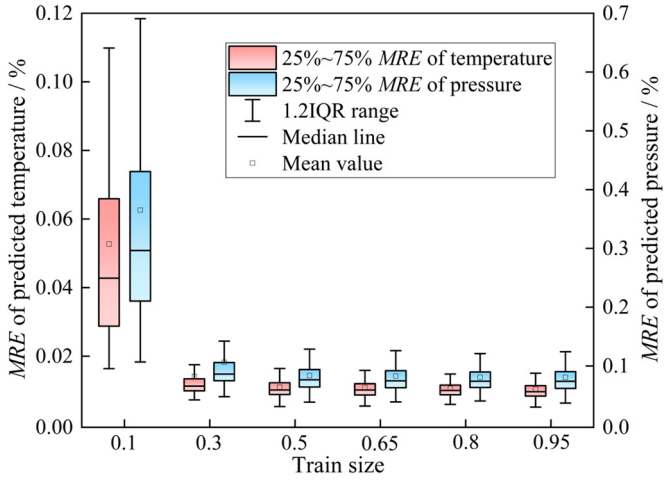

Fig. 17. Predicted fields of different train sizes.

large gradient areas at the leading and trailing edge of the blade. The predicted relative error of Dual-CNN model for efficiency and torque is lower than that of GPR model and ANN model, and its error is within an acceptable range of optimization.

(2) Based on Dual-CNN, multi-objective optimization is performed with efficiency and torque as the objective function, and the Pareto solution is obtained considering 11 kinds of importance proportion w. Taking the condition where efficiency and torque share respectively 50% importance as an example, the efficiency and power of the optimized blade profile are respectively 93.43% and 16.12 MW.

(3) Comparing the performance prediction and field reconstruction accuracy of six train sizes of 0.1, 0.3, 0.5, 0.65, 0.8, 0.95, it can be concluded that the sampling of 1500 cases enables Dual-CNN to achieve favorable effect of field reconstruction and performance prediction. The predicted mean relative error and the corresponding standard deviation are relatively small. The proposed Dual-CNN can serve as an efficient analysis tool for the turbine performance instead of CFD software.

Declaration of competing interest

The authors declare that they have no known competing financial interests or personal relationships that could have appeared to influence the work reported in this paper.

Acknowledgements

This work was support by 111 Project of Chinese Ministry of Education (Grant No. B16038).

References

[1] S.N. Skinner, H. Zare-Behtash, State-of-the-art in aerodynamic shape optimisation methods, Appl. Soft Comput. 62 (2018) 933–962, https://doi.org/10.1016/j.asoc.2017.09.030.

[2] L. Zhoujie, G.K.W. Kenway, C. Paige, J.R.R.A. Martins, Automatic differentiation adjoint of the Reynolds-averaged Navier-Stokes equations with a turbulence model, in: 21st AIAA Computational Fluid Dynamics Conference, 2013, p. 24.

[3] G.L.O. Halila, J.R.R.A. Martins, K.J. Fidkowski, Adjoint-based aerodynamic shape optimization including transition to turbulence effects, Aerosp. Sci. Technol. 107 (2020), https://doi.org/10.1016/j.ast.2020.106243.

[4] A. Rubino, S. Vitale, P. Colonna, M. Pini, Fully-turbulent adjoint method for the unsteady shape optimization of multi-row turbomachinery, Aerosp. Sci. Technol. 106 (2020), https://doi.org/10.1016/j.ast.2020.106132.

[5] A.C. Marta, C.A. Mader, J. Martins, E. Van der Weide, J.J. Alonso, A methodology for the development of discrete adjoint solvers using automatic differentiation tools, Int. J. Comput. Fluid Dyn. 21 (2007) 307–327, https://doi.org/10.1080/10618560701678647.

[6] R.W. Lei, J.Q. Bai, D.Y. Xu, Aerodynamic optimization of civil aircraft with wing-mounted engine jet based on adjoint method, Aerosp. Sci. Technol. 93 (2019) 14, https://doi.org/10.1016/j.ast.2019.07.018.

[7] G.K.W. Kenway, J. Martins, Multipoint high-fidelity aerostructural optimization of a transport aircraft configuration, J. Aircr. 51 (2014) 144–160, https://doi.org/10.2514/1.C032150.

[8] J. Martins, J.J. Alonso, J.J. Reuther, A coupled-adjoint sensitivity analysis method for high-fidelity aero-structural design, Optim. Eng. 6 (2005) 33–62, https://doi.org/10.1023/b:Opte.0000048536.47956.62.

[9] M. Nemec, D.W. Zingg, T.H. Pulliam, Multipoint and multi-objective aerodynamic shape optimization, AIAA J. 42 (2004) 1057–1065, https://doi.org/10.2514/1.10415.

[10] A. Kusiak, H.Y. Zheng, Optimization of wind turbine energy and power factor with an evolutionary computation algorithm, Energy 35 (2010) 1324–1332, https://doi.org/10.1016/j.energy.2009.11.015.

[11] S. Mehrnia, K. Miyagawa, J. Kusaka, Y. Nakamura, Radial turbine optimization under unsteady flow using nature-inspired algorithms, Aerosp. Sci. Technol. 103 (2020) 15, https://doi.org/10.1016/j.ast.2020.105903.

[12] B. Yang, Q. Xu, L. He, L.H. Zhao, C.G. Gu, P. Ren, A novel global optimization algorithm and its application to airfoil optimization, J. Turbomach. 137 (2015) 10, https://doi.org/10.1115/1.4028712.

[13] J. Cruz, I. Amaya, R. Correa, Optimal rectangular microchannel design, using simulated annealing, unified particle swarm and spiral algorithms, in the presence of spreading resistance, Appl. Therm. Eng. 84 (2015) 126–137, https://doi.org/10.1016/j.applthermaleng.2015.03.049.

[14] N.V. Queipo, R.T. Haftka, W. Shyy, T. Goel, R. Vaidyanathan, P.K. Tucker, Surrogate-based analysis and optimization, Prog. Aerosp. Sci. 41 (2005) 1–28, https://doi.org/10.1016/j.paerosci.2005.02.001.

[15] A.I.J. Forrester, A.J. Keane, Recent advances in surrogate-based optimization, Prog. Aerosp. Sci. 45 (2009) 50–79, https://doi.org/10.1016/j.paerosci.2008.11.001.

[16] L. Leifsson, S. Koziel, Y.A. Tesfahunegn, Multiobjective aerodynamic optimization by variable-fidelity models and response surface surrogates, AIAA J. 54 (2016) 531–541, https://doi.org/10.2514/1.J054128.

[17] D.J.J. Toal, A.J. Keane, Efficient multipoint aerodynamic design optimization via cokriging, J. Aircr. 48 (2011) 1685–1695, https://doi.org/10.2514/1.C031342.

[18] C.X. Li, J. Wang, Z.D. Guo, L.M. Song, J. Li, Aero-mechanical multidisciplinary optimization of a high speed centrifugal impeller, Aerosp. Sci. Technol. 95 (2019) 15, https://doi.org/10.1016/j.ast.2019.105452.

[19] B. Li, C.-w. Gu, X.-t. Li, T.-q. Liu, Numerical optimization for stator vane settings of multi-stage compressors based on neural networks and genetic algorithms, Aerosp. Sci. Technol. 52 (2016) 81–94, https://doi.org/10.1016/j.ast.2016.02.024.

[20] C.W. Fei, W.Z. Tang, G.C. Bai, Novel method and model for dynamic reliability optimal design of turbine blade deformation, Aerosp. Sci. Technol. 39 (2014) 588–595, https://doi.org/10.1016/j.ast.2014.07.003.

[21] T. Baklacioglu, O. Turan, H. Aydin, Dynamic modeling of exergy efficiency of turboprop engine components using hybrid genetic algorithm-artificial neural networks, Energy 86 (2015) 709–721, https://doi.org/10.1016/j.energy.2015.04.025.

[22] J. Sarshar, S.S. Moosapour, M. Joorabian, Multi-objective energy management of a micro-grid considering uncertainty in wind power forecasting, Energy 139 (2017) 680–693, https://doi.org/10.1016/j.energy.2017.07.138.

[23] Z. Yao, S. WoongJe, D. Mavris, Application of convolutional neural network to predict airfoil lift coefficient, in: 2018 AIAA/ASCE/AHS/ASC Structures, Structural Dynamics, and Materials Conference, 2018, p. 9.

[24] M. Moret, A. Delecourt, H. Moustapha, A.-I. Abenhaim, F. Garnier, Automated thermal and stress preliminary analyses applied to a turbine rotor, Aerosp. Sci. Technol. 63 (2017) 123–131, https://doi.org/10.1016/j.ast.2016.12.013.

[25] Y.H. Yu, L.E. Chen, F.R. Sun, C. Wu, Neural-network based analysis and prediction of a compressor's characteristic performance map, Appl. Energy 84 (2007) 48–55, https://doi.org/10.1016/j.apenergy.2006.04.005.

[26] J. Marx, S. Gantner, J. Stading, J. Friedrichs, A machine learning based approach of performance estimation for high-pressure compressor airfoils, in: ASME, Amer Soc Mechanical Engineers, New York, 2018.

[27] T.Y. Liu, Y.Z. Li, Y.H. Xie, D. Zhang, Deep learning for nanofluid field reconstruction in experimental analysis, IEEE Access 8 (2020) 64692–64706, https://doi.org/10.1109/access.2020.2979794.

[28] T.Y. Liu, Y.Z. Li, Q. Jing, Y.H. Xie, D. Zhang, Supervised learning method for the physical field reconstruction in a nanofluid heat transfer problem, Int. J. Heat Mass Transf. 165 (2021) 24, https://doi.org/10.1016/j.ijheatmasstransfer.2020.120684.

[29] Y. Ahn, S.J. Bae, M. Kim, S.K. Cho, S. Baik, J.I. Lee, J.E. Cha, Review of supercritical CO2 power cycle technology and current status of research and development, Nucl. Eng. Technol. 47 (2015) 647–661, https://doi.org/10.1016/j.net.2015.06.009.

[30] F. Crespi, G. Gavagnin, D. Sanchez, G.S. Martinez, Supercritical carbon dioxide cycles for power generation: a review, Appl. Energy 195 (2017) 152–183, https://doi.org/10.1016/j.apenergy.2017.02.048.

[31] C. Wu, S.S. Wang, J. Li, Exergoeconomic analysis and optimization of a combined supercritical carbon dioxide recompression Brayton/organic flash cycle

for nuclear power plants, Energy Convers. Manag. 171 (2018) 936–952, https://doi.org/10.1016/j.enconman.2018.06.041.
[32] M. Valdes, R. Abbas, A. Rovira, J. Martin-Aragon, Thermal efficiency of direct, inverse and sCO(2) gas turbine cycles intended for small power plants, Energy 100 (2016) 66–72, https://doi.org/10.1016/j.energy.2016.01.072.
[33] F. Jacob, A.M. Rolt, J.M. Sebastiampillai, V. Sethi, M. Belmonte, P. Cobas, Performance of a supercritical CO2 bottoming cycle for aero applications, Appl. Sci. 7 (2017), https://doi.org/10.3390/app7030255.
[34] J.F. Wang, Z.X. Sun, Y.P. Dai, S.L. Ma, Parametric optimization design for supercritical CO2 power cycle using genetic algorithm and artificial neural network, Appl. Energy 87 (2010) 1317–1324, https://doi.org/10.1016/j.apenergy.2009.07.017.
[35] Q.H. Deng, D. Wang, H. Zhao, W.T. Huang, S. Shao, Z.P. Feng, Study on performances of supercritical CO2 recompression Brayton cycles with multi-objective optimization, Appl. Therm. Eng. 114 (2017) 1335–1342, https://doi.org/10.1016/j.applthermaleng.2016.11.055.
[36] M.D. Zeiler, G.W. Taylor, R. Fergus, Adaptive deconvolutional networks for mid and high level feature learning, in: 2011 IEEE International Conference on Computer Vision, IEEE, IEEE, New York, 2011, pp. 2018–2025.
[37] M.D. Zeiler, R. Fergus, Visualizing and understanding convolutional networks, in: D. Fleet, T. Pajdla, B. Schiele, T. Tuytelaars (Eds.), Computer Vision - ECCV 2014, Pt I, Springer International Publishing Ag, Cham, 2014, pp. 818–833, vol. 8689.
[38] D.P. Kingma, J.B. Adam, A method for stochastic optimization, arXiv preprint, arXiv:1412.6980, 2014.
[39] A. Paszke, S. Gross, F. Massa, A. Lerer, J. Bradbury, G. Chanan, T. Killeen, Z.M. Lin, N. Gimelshein, L. Antiga, A. Desmaison, A. Kopf, E. Yang, Z. DeVito, M. Raison, A. Tejani, S. Chilamkurthy, B. Steiner, L. Fang, J.J. Bai, S. Chintala, PyTorch: an imperative style, high-performance deep learning library, in: H. Wallach, H. Larochelle, A. Beygelzimer, F. d'Alche-Buc, E. Fox, R. Garnett (Eds.), Advances in Neural Information Processing Systems 32, Neural Information Processing Systems (Nips), La Jolla, 2019, vol. 32.
[40] P. Ma, T. Du, W. Matusik, Efficient continuous Pareto exploration in multi-task learning, arXiv preprint, arXiv:2006.16434, 2020.
[41] H. Wang, D.Y. Yeung, A survey on Bayesian deep learning, arXiv preprint, arXiv:1604.01662, 2016.
[42] J.R. Gardner, G. Pleiss, D. Bindel, K.Q. Weinberger, A.G. Wilson, GPyTorch: blackbox matrix-matrix Gaussian process inference with GPU acceleration, in: S. Bengio, H. Wallach, H. Larochelle, K. Grauman, N. Cesa-Bianchi, R. Garnett (Eds.), Advances in Neural Information Processing Systems 34, 2018, vol. 34.
[43] D. Luo, Y. Liu, X.J. Sun, D.G. Huang, The design and analysis of supercritical carbon dioxide centrifugal turbine, Appl. Therm. Eng. 127 (2017) 527–535, https://doi.org/10.1016/j.applthermaleng.2017.08.039.
[44] Y.Q. Wang, J.X. Li, D. Zhang, Y.H. Xie, Numerical investigation on aerodynamic performance of SCO2 and air radial-inflow turbines with different solidity structures, Appl. Sci. 10 (2020) 18, https://doi.org/10.3390/app10062087.
[45] M. Odabaee, E. Sauret, K. Hooman, CFD simulation of a supercritical carbon dioxide radial-inflow turbine, comparing the results of using real gas equation of estate and real gas property file, Appl. Mech. Mater. 846 (2016) 85–90, https://doi.org/10.4028/www.scientific.net/AMM.846.85.
[46] S.G. Kim, J. Lee, Y. Ahn, J.I. Lee, Y. Addad, B. Ko, CFD investigation of a centrifugal compressor derived from pump technology for supercritical carbon dioxide as a working fluid, J. Supercrit. Fluids 86 (2014) 160–171, https://doi.org/10.1016/j.supflu.2013.12.017.
[47] A. Ameli, A. Afzalifar, T. Turunen-Saaresti, J. Backman, Centrifugal compressor design for near-critical point applications, J. Eng. Gas Turbines Power 141 (2019), https://doi.org/10.1115/1.4040691.